ELSEVIER

Chemical Engineering Journal 85 (2002) 69–79

Chemical Engineering Journal

www.elsevier.com/locate/cej

Theoretical study of the application of porous membrane reactor to oxidative dehydrogenation of *n*-butane

Suttichai Assabumrungrat [a,*], Tavorn Rienchalanusarn [a], Piyasan Praserthdam [a], Shigeo Goto [b]

[a] *Petrochemical Engineering Laboratory, Department of Chemical Engineering, Chulalongkorn University, Bangkok 10330, Thailand*
[b] *Department of Chemical Engineering, Nagoya University, Chikusa, Nagoya 464-8603, Japan*

Received 20 October 2000; accepted 24 February 2001

Abstract

This paper is the theoretical study of the oxidative dehydrogenation of *n*-butane in porous membrane reactors. Performance of the membrane reactors was compared with that of conventional fixed-bed reactors. The porous membrane was employed to add oxygen to the reaction side in a controlled manner so that the reaction could take place evenly.

Mathematical models for the fixed-bed reactor and the membrane reactor were developed considering non-isothermal condition and both radial heat and mass dispersion. From this study, it was found that the hot spot problem was pronounced particularly near the entrance of the conventional fixed-bed reactor. In addition, the assumption of plug flow condition did not adequately represent the reaction system. The effect of radial dispersion must be taken into account in the modelling.

The use of the porous membrane to control the distribution of oxygen feed to the reaction side could significantly reduce the hot spot temperature. The results also showed that there were optimum feed ratios of air/*n*-butane for both the fixed-bed reactors and the membrane reactors. The membrane reactor outperformed the fixed-bed reactor at high values of the ratio. In addition, there was an optimum membrane reactor size. When the reactor size was smaller than the optimum value, the increased reactor size increased the reaction and heat generation and, consequently, the conversion and the selectivity to C_4 increased. However, when the reactor size was larger than the optimum value, oxygen could not reach the reactant near the stainless steel wall. It was consumed to react with the product, C_4. As a result, the yield dropped. Finally, it was found that the increase of wall temperature increased the yield and that the feed air temperature could help control the temperature profile of the reaction bed along the reactor length.

Keywords: Oxidative dehydrogenation; Inert membrane reactor; Hot spot temperature; Radial dispersion

1. Introduction

The concept of membrane reactor in which reaction and separation are incorporated in a single unit operation has attracted many researchers' interests for the past several decades. There are a number of reviews addressing the development of the membrane reactor for catalytic reactions taking place at high temperature [1–5]. Major application areas of membrane reactor can be classified into two types; i.e. yield enhancement and selectivity enhancement. The former area is mainly applied to reactions suffering from equilibrium conversions such as dehydrogenation reactions, decomposition and production of synthesis gas. The latter area is mainly applied to series-parallel reactions such as partial oxidation, partial hydrogenation, oxidative coupling and oxidative dehydrogenation by controlled addition of a reactant through a membrane to the reaction zone so that the partial pressure in the reaction zone is kept at low value.

Oxidative dehydrogenation, which is the reaction of interest in this study, is another alternative to produce unsaturated hydrocarbons. Unlike direct removal of hydrogen from saturated hydrocarbon in a dehydrogenation reaction, the reaction is unlimited by thermodynamic equilibrium, energy saving and tolerated to catalyst deactivation. However, the reaction encounters some drawbacks of low selectivity, formation of hot spot and problem of flammability limits. One approach to improve the performance of the reaction system has been focused on the use of non-traditional reactors such as fixed-bed reactors with distributed feed points, monolith reactors, catalytic membrane reactors and inert membrane reactors. The oxidative dehydrogenation of propane in a fixed bed reactor and a monolith reactor was studied and found that as the residence time or propane conversion increased, the selectivity to propylene was almost constant in the monolith reactor unlike the fixed bed reactor

* Corresponding author.
E-mail address: fchsas@eng.chula.ac.th (S. Assabumrungrat).

1385-8947/02/$ – see front matter
PII: S1385-8947(01)00146-2

Nomenclature

a	Knudsen parameter (mol $K^{1/2}$/(m s kPa))
A_C	cross section area (m^2)
A_{P1}	surface area of reactor at r_1 (m^2)
A_{P2}	surface area of reactor at r_2 (m^2)
A_{P3}	surface area of reactor at r_3 (m^2)
b	viscous parameter (mol K/(m kPa))
C_i	concentration (mol/m^3)
C_{pi}	heat capacity (J/(mol K))
d_p	particle diameter (m)
D	equivalent diameter (m)
D_{er}	effective radial diffusion (m^2/s)
D_{ij}	diffusion coefficient of binary gas (m^2/s)
$D_{i,m}$	diffusion coefficient of gas mixture (m^2/s)
E_{ai}	activity coefficient (J/mol)
F_i	molar flow rate (mol/s)
h_{bed}	film heat transfer in catalyst bed (W/(m^2 K))
h_{ex}	film heat transfer in tube (W/(m^2 K))
H_i	enthalpy (J/mol)
ΔH_{ri}	heat of reaction of reaction i (J/mol)
J	molar flux (mol/(m^2 s))
k_i	rate constant (mol/(kg s))
k_M	thermal conductivity of membrane (W/(m K))
k_{ss}	thermal conductivity of stainless steel (W/(m K))
L	reactor length (m)
M	molecular weight (g/mol)
Nu_{bed}	Nusselt number in catalyst bed
Nu_{ex}	Nusselt number in tube
P	pressure (kPa)
Pe_r	radial peclet number
Pr	Prandtl number
q_i	molar flow rate of permeate gas i per unit length (mol/(s m))
r	radial distance (m)
r_i	rate of reaction of species i (mol/(kg s))
r_1, r_2	reactor diameter (m)
r_3, r_4	reactor diameter (m)
R_{gas}	gas constant (J/(mol K))
R_i	rate of reaction of reaction i (mol/(kg s))
Re	Reynolds number
Re_p	packed bed Reynolds number
Sc	Schmidt number
t	time (s)
T	temperature (K)
T_f	feed temperature (K)
T_j	reactor wall temperature
u	gas velocity (m/s)
U_i	parameter in Eq. (A.4)
U_M	overall heat transfer coefficient through membrane (W/(m^2 K))
U_{ss}	overall heat transfer coefficient through stainless steel (W/(m^2 K))
y_i	mole fraction
z	length (m)

Greek symbols

ε	porosity
η	dipole moment (debye)
η_r	dimensionless dipole moment
λ_0	non-selective oxidation site
λ	thermal conductivity (W/(m K))
λ_{er}	effective radial thermal conductivity (W/(m K))
λ_{er}^0	static effective radial thermal conductivity (W/(m K))
λ_{er}^t	dynamic effective radial thermal conductivity (W/(m K))
μ	viscosity (P)
ν_i	stoichiometric coefficient
θ_0	selective oxidation site
ρ	density of gas (kg/m^3)
ρ_B	density of catalyst (kg/m^3)

Subscript

0	inlet condition
c	critical condition
g	gas
m	mixture gas
r	reduce
s	shell side
t	tube side
T	total

Superscript

s	shell side
t	tube side

whose selectivity decreased rapidly [6]. In addition, when oxygen was a limiting reactant, the selectivity to propylene is higher than the case of excess oxygen. The performance of three types of reactors; i.e. fixed bed, monolith and catalytic membrane reactors (CMR) was investigated [7,8]. CMR gave slightly higher selectivity to propylene than the monolith reactor because of the higher HC/O_2 ratio.

The use of an inert membrane reactor has drawn a number of interests in the recent years. Some researches pointed out the superior yield of inert membrane reactor (IMR) over CMR [9,10]. A number of oxidative dehydrogenation reactions have been investigated in IMR, for example, the oxidative dehydrogenation of ethane [11–13], propane [10] and *n*-butane [14,15]. All researchers found that the distribution of O_2 feed by using membranes increased the reactor performance. The controlled addition of O_2 does not only improve the selectivity but also avoids the explosion mixture. As a result, wider ranges of operating conditions can be performed. The IMRs have be employed to other selective oxidation reactions such as the oxidative coupling of methane [16–18], partial oxidation of butane to maleic

anhydride [19] and the epoxidation of ethylene to ethylene oxide [20].

In this study, the oxidative dehydrogenation of *n*-butane in inert membrane reactors is considered. There are only a few papers addressing the use of membrane reactor to this reaction [14,15,21]. An experimental investigation was carried out to show that the formation of hot spots was decreased considerably with the use of inert membrane reactor [15]. Later, the same investigators developed a simple mathematical model assuming plug-flow condition to describe the system [14]. The beneficial effect on the improvement of reactor safety and operability was examined.

In this paper, two-dimensional models taking into account the radial dispersion of energy and mass which have not been studied extensively in the literature are developed to study the performance of the inert membrane reactor (IMR) compared with that of a fixed bed reactor and the significance of the radial dispersion in this system. Various operating conditions and design parameters are varied to investigate their effects on the reactor performance.

2. Mathematical modelling

The oxidative dehydrogenation of *n*-butane to butene and butadiene is accompanied by side reactions of deep oxidation of products and reactant to CO and CO_2. The reaction networks are shown in Fig. 1. Reactions 1, 2 and 3 in this scheme refer, respectively, to the formation of 1-butene, *cis*-2-butene and *trans*-2-butene from *n*-butane. However, three isomers of 1-butene, *trans*-2-butene and *cis*-2-butene are lumped as C_4H_8 in reactions 7, 8 and 9. The kinetic data over V/MgO catalysts obtained from a literature can be expressed by Mars-van Krevelen model as shown in Table 1 [21]. The kinetic expressions were obtained from the experimental results under the following conditions; i.e. temperature between 748–823 K; oxygen concentration of 2–10%; hydrocarbon concentration of 2–10%; water concentration of 0–3% and CO_2 concentration of 0–3%.

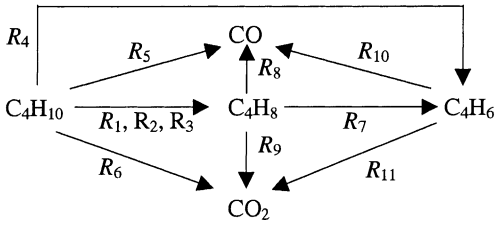

Fig. 1. Reaction scheme proposed by Tellez et al. [21].

The reaction rate constant (k_i) is given by $k_i = k_{i0} \times \exp(-(E_{ai}/R)(1/T - 1/T_0))$. The reference temperature, T_0 is equal to 773 K. The V/MgO catalyst (24 wt.% of V_2O_5) was packed in an annulus side between a tubular γ-Al_2O_3 membrane and a stainless steel shell for the membrane reactor while it was packed in a stainless steel tube for the fixed bed reactor. The gas permeation through the membrane is based on the permeation data of gases through a commercial "Membralox" membrane. The expression for gas permeation rate per unit membrane length, q_i, is as follows [22].

$$q_i = \frac{a(P_t y_{i,t} - P_s y_{i,s})}{\sqrt{M_i T}} + \frac{b y_{i,t}(P_t^2 - P_s^2)}{2\mu_m T} \quad (1)$$

where a and b are Knudsen and viscous flow parameters, respectively; $y_{i,s}$ and $y_{i,t}$ are mole fractions of species i in the shell side and the tube side respectively.

Two mathematical models are developed for the fixed-bed reactor and the membrane reactor based on the following assumptions: steady-state operation, negligible pressure drop, ideal behavior of gases, constant reactor wall temperature, negligible diffusion resistance of the particle of catalyst, negligible axial dispersion and catalytically inactive membrane. The radial diffusion models take into account the non-isothermal condition and radial heat and mass transfer were developed as follows.

Table 1
Rate expression and kinetic parameters determined by Tellez et al. [21][a]

Reactions	Rate expression	$k_{i0} \times 10^3$ (mol/s kg)	E_{ai} (kJ/mol)
$C_4H_{10} + X_0 \rightarrow$ 1-$C_4H_8 + H_2O + X$	$R_1 = k_1 \times P_{C_4H_{10}} \times \theta_0$	62.33	144.9
$C_4H_{10} + X_0 \rightarrow$ *Trans*-2-$C_4H_8 + H_2O + X$	$R_2 = k_2 \times P_{C_4H_{10}} \times \theta_0$	32.83	142.7
$C_4H_{10} + X_0 \rightarrow$ *Cis*-2-$C_4H_8 + H_2O + X$	$R_3 = k_3 \times P_{C_4H_{10}} \times \theta_0$	39.67	139.1
$C_4H_{10} + 2X_0 \rightarrow C_4H_6 + 2H_2O + 2X$	$R_4 = k_4 \times P_{C_4H_{10}} \times \theta_0$	30.83	148.5
$C_4H_{10} + 9Z_0 \rightarrow 4CO + 5H_2O + 9Z$	$R_5 = k_5 \times P_{C_4H_{10}} \times \theta_0$	9.17	175.5
$C_4H_{10} + 13Z_0 \rightarrow 4CO_2 + 5H_2O + 13Z$	$R_6 = k_6 \times P_{C_4H_{10}} \times \theta_0$	25.83	138.4
$C_4H_8 + X_0 \rightarrow C_4H_6 + H_2O + X$	$R_7 = k_7 \times P_{C_4H_8} \times \theta_0$	685.00	164.7
$C_4H_8 + 8Z_0 \rightarrow 4CO + 4H_2O + 8Z$	$R_8 = k_8 \times P_{C_4H_8} \times \theta_0$	32.33	146.2
$C_4H_8 + 12Z_0 \rightarrow 4CO_2 + 4H_2O + 12Z$	$R_9 = k_9 \times P_{C_4H_8} \times \lambda_0$	115.67	107.2
$C_4H_6 + 7Z_0 \rightarrow 4CO + 3H_2O + 7Z$	$R_{10} = k_{10} \times P_{C_4H_6} \times \lambda_0$	118.17	146.6
$C_4H_6 + 11Z_0 \rightarrow 4CO_2 + 3H_2O + 11Z$	$R_{11} = k_{11} \times P_{C_4H_6} \times \lambda_0$	435	102.0
$O_2 + 2X \rightarrow 2X_0$	$R_{12} = k_{12} \times P_{O_2} \times (1 - \theta_0)$	2995	114.5
$O_2 + 2Z \rightarrow 2Z_0$	$R_{13} = k_{13} \times P_{O_2} \times (1 - \lambda_0)$	3255	5.5

[a] where $k_i = k_{i0}\, e^{-E_{ai}(1/T - 1/T_0)}$, $T_0 = 773$ K and $\theta_0 = 2k_{12}P_{O_2}/\{2k_{12}P_{O_2} + (k_1 + k_2 + k_3 + 2k_4)P_{C_4H_{10}} + k_7 \times P_{C_4H_8}\}$; $\lambda_0 = 2k_{13}P_{O_2}/\{2k_{13}P_{O_2} + (9k_5 + 13k_6)P_{C_4H_{10}} + (8k_8 + 12k_9)P_{C_4H_8} + (7k_{10} + 11k_{11})P_{C_4H_6}\}$.

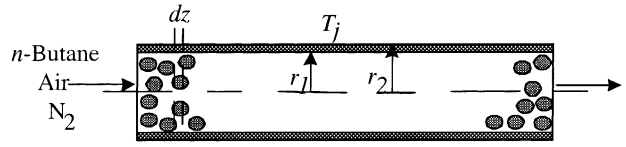

Fig. 2. Schematic diagram of a fixed-bed reactor.

2.1. Fixed-bed reactor (FBR)

Fig. 2 shows the schematic diagram of the fixed-bed reactor. By performing the mass balance and energy balance, the following equations can be obtained.

2.1.1. Mass balances of species i

$$\frac{1}{A_C}\frac{\partial F_i}{\partial z} = D_{er}\left(\frac{1}{r}\frac{\partial C_i}{\partial r} + \frac{\partial^2 C_i}{\partial r^2}\right) + \rho_B R_i \tag{2}$$

B.C.

$$z = 0, \quad C_i = C_{i,0} \quad \text{for all } r$$

$$r = 0, \quad \frac{\partial C_i}{\partial r} = 0 \quad \text{for all } z$$

$$r = r_1, \quad \frac{\partial C_i}{\partial r} = 0 \quad \text{for all } z$$

2.1.2. Energy balance

$$\frac{\partial T}{\partial z} = \frac{A_C}{\sum_{i=1}^{n} F_i C_{pi}}\lambda_{er}\left(\frac{1}{r}\frac{\partial T}{\partial r} + \frac{\partial^2 T}{\partial r^2}\right) + \rho_B \sum_{i=1}^{n}(-\Delta H_{ri} R_i)\frac{A_C}{\sum_{i=1}^{n} F_i C_{pi}} \tag{3}$$

B.C.

$$z = 0, \quad T = T_0 \quad \text{for all } r$$

$$r = 0, \quad \frac{\partial T}{\partial r} = 0 \quad \text{for all } z$$

$$r = r_1, \quad -\lambda_{er}\frac{\partial T}{\partial r} = U_{ss_{er}}(T_{r=r_1} - T_j) \quad \text{for all } z$$

2.2. Inert membrane reactor (IMR)

Fig. 3 shows the schematic diagram of a membrane reactor. By performing the mass balance and energy balance, the following equations can be obtained. It is noted that the radial dispersion is considered only in the packed-bed of catalyst. The radial effect is assumed to be negligible in the oxygen feed side.

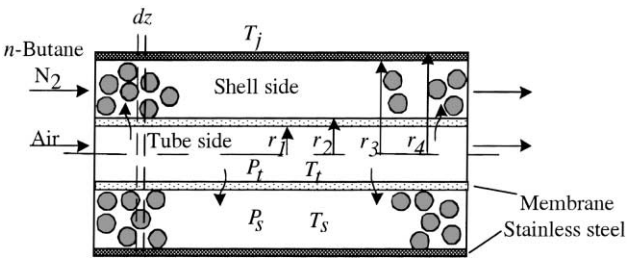

Fig. 3. Schematic diagram of inert membrane reactor.

2.2.1. Mass balances of species i

Shell side

$$\frac{1}{A_{C_s}}\frac{\partial F_i^s}{\partial z} = D_{er}^s\left(\frac{1}{r}\frac{\partial C_i^s}{\partial r} + \frac{\partial^2 C_i^s}{\partial r^2}\right) + \rho_B R_i \tag{4}$$

B.C.

$$z = 0, \quad C_i^s = C_{i,0}^s, \quad F_i^s = F_{i,0}^s \quad \text{for all } r$$

$$r = r_2, \quad \frac{\partial C_i^s}{\partial r} = \frac{P_s}{R_{gas}}\frac{\partial}{\partial r}\left(\frac{F_i^s}{\sum_j F_j^s T_s}\right) = \frac{1}{D_{er}^s 2\pi r_2} q_i \quad \text{for all } z$$

$$r = r_3, \quad \frac{\partial C_i^s}{\partial r} = 0 \quad \text{for all } z$$

P_t and P_s are total pressure at tube and shell side, respectively.

Tube side

$$\frac{dF_i^t}{dz} = -q_i \tag{5}$$

2.2.2. Energy balance

Shell side

$$\frac{\partial T_s}{\partial z} = \frac{\pi(r_3^2 - r_2^2)}{\sum_{i=1}^{n} F_i^s C_{pi}}\lambda_{er}^s\left(\frac{1}{r}\frac{\partial T_s}{\partial r} + \frac{\partial^2 T_s}{\partial r^2}\right) + \rho_B \sum_{i=1}^{n}(-\Delta H_{ri} R_i)\frac{\pi(r_3^2 - r_2^2)}{\sum_{i=1}^{n} F_i^s C_{pi}} \tag{6}$$

B.C.

$$z = 0, \quad T_s = T_{s,0} \quad \text{for all } r$$

$$r = r_2, \quad -\lambda_{er}^s\frac{\partial T_s}{\partial r} = U_M(T_{t_{r=r_1}} - T_{s_{r=r_2}}) + \sum_{i=1}^{n}\left(\frac{1}{2\pi r_2} q_i H_i\right) \quad \text{for all } z$$

$$r = r_3, \quad -\lambda_{s_{er}}\frac{\partial T_s}{\partial r} = U_{ss_{er}}(T_{s_{r=r_3}} - T_j) \quad \text{for all } z$$

Tube side

$$\sum_{i=1}^{n}(F_i^t C_{pi})\frac{dT_t}{dz} = U_M 2\pi r_1(T_s - T_t) - \sum_{i=1}^{n} H_i q_i \tag{7}$$

When the differential terms with respect to the radius, r, are omitted in Eqs. (2)–(7), plug flow models can be derived for both the fixed bed reactor and the membrane reactor.

The finite difference method was used to solve the radial diffusion model while the fourth order Runge–Kutta method was employed to solve the set of nonlinear equations of the plug flow model. The problem on numerical stability or convergence of the simulation could be conquered by changing increments of both radial and axial directions for the radial diffusion model.

Table 2
The standard condition and range of parameters in study

Parameters	Standard condition	Value in study
i.d. of fixed bed reactor (m)	0.006	0.006–0.008
o.d. of fixed bed reactor (m)	0.009	0.009–0.011
i.d. of membrane tube (m)	0.007	0.007
o.d. of membrane tube (m)	0.010	0.010
i.d. of stainless steel shell (m)	0.0117	0.0117–0.051
o.d. of stainless steel shell (m)	0.0147	0.0147–0.054
Total molar flow rate (mol/s)	4.464×10^{-4}	4.464×10^{-4}
Inert introgen flow rate (mol/s)	2.976×10^{-4}	2.976×10^{-4}
Reactant flow rate (mol/s)	1.488×10^{-4}	1.488×10^{-4}
Air to *n*-butane ratio in reactant feed	8	1–15
Pressure (kPa)	101.3	101.3
Feed temperature (K)	773	773
Coolant temperature (K)	773	753–803
Catalyst size (μm)	250	250
Packed bed density (kg/m^3)	700	700
Packed bed porosity	0.4	0.4
Reactor diameter (m)	0.006	0.006–0.05
Knudsen parameter a (mol K^{12}/m s kPa)	4.8×10^{-3}	4.8×10^{-3}
Viscous parameter b (mol K/m kPa)	1×10^{-12}	1×10^{-12}

3. Results and discussion

The standard operating condition and the reactor configuration used in this study for both fixed-bed reactor and inert membrane reactors are given in Table 2.

3.1. Performance of fixed-bed reactor

3.1.1. Effect of reaction temperature

Fig. 4 shows the performance of the fixed-bed reactor at various operating temperature. The conversion of *n*-butane and oxygen and selectivity to butene, butadiene, total dehydrogenated C_4 products (summation value of the selectivity to butene and butadiene), carbon dioxide and carbon monoxide were presented. The conversion of oxygen is always 100% independently of temperature. This means that oxygen is the limiting component in this condition. The increase of the reaction temperature increases the conversion of *n*-butane but decreases the selectivity to carbon dioxide and butene. The selectivity to carbon monoxide is almost constant. However, the selectivity to butadiene is more favorable at high temperature than the selectivity to butene, resulting in the increased selectivity to the total dehydrogenated C_4 products. It can be concluded that the desired products C_4 are favorable at high operating temperature. This similar effect was also reported by other workers [15,23].

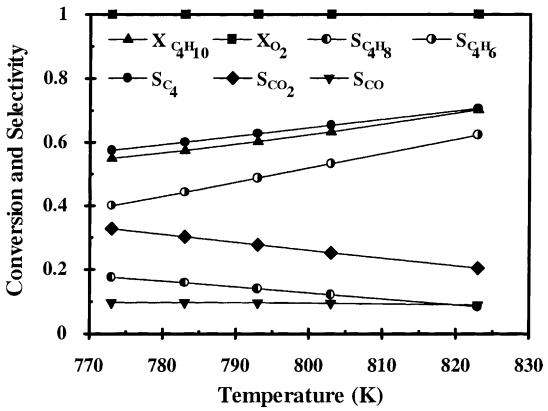

Fig. 4. Effect of reaction temperature in the fixed bed reactor (isothermal plug flow model, air/*n*-butane ratio = 8, $d = 0.006$ m, feed flow rate of *n*-butane 1.65×10^{-5} mol/s, T_f and T_j=773 K, $W/F_{C_4H_{10}}$=160 kg s/ mol).

3.1.2. Comparison between plug flow model and radial diffusion model

Fig. 5 compares the results of the fixed-bed reactor between two models; i.e. the plug flow model and the radial diffusion model. The filled symbols show the values from the radial diffusion model while the empty symbols show the values from the plug flow model. When $W/F_{C_4H_{10}}$ increases the conversions of *n*-butane and oxygen increase while the selectivity to butene decreases and reaches the asymptote. On the contrary, the selectivity to butadiene and carbon oxides shows opposite results. This is because butene is a primary reaction product while butadiene and carbon oxides are both primary and secondary reaction products. The comparison between the filled symbols and the empty symbols shows that the assumption of plug flow condition did not adequately represent the system. The effect of the radial dispersion in the modelling of the process should be taken into account.

Fig. 6 shows temperature profiles of both radial and axial directions in the radial diffusion model. Since the oxidative dehydrogenation is a highly exothermic reaction and the reaction takes place mainly near the entrance of the reactor,

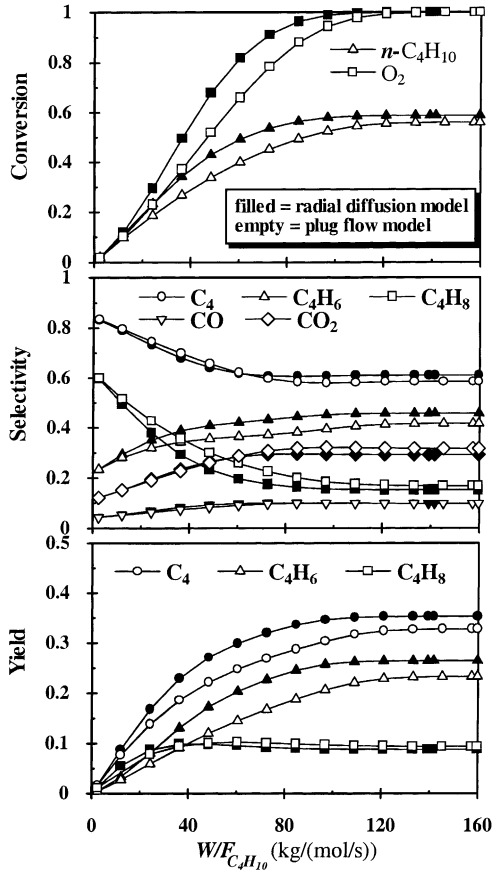

Fig. 5. Conversion selectivity and yield of plug flow and radial diffusion model (air/*n*-butane ratio = 8, $d = 0.006$ m, feed flow rate of *n*-butane = 1.653×10^{-5} mol, T_f and $T_j = 773$ K).

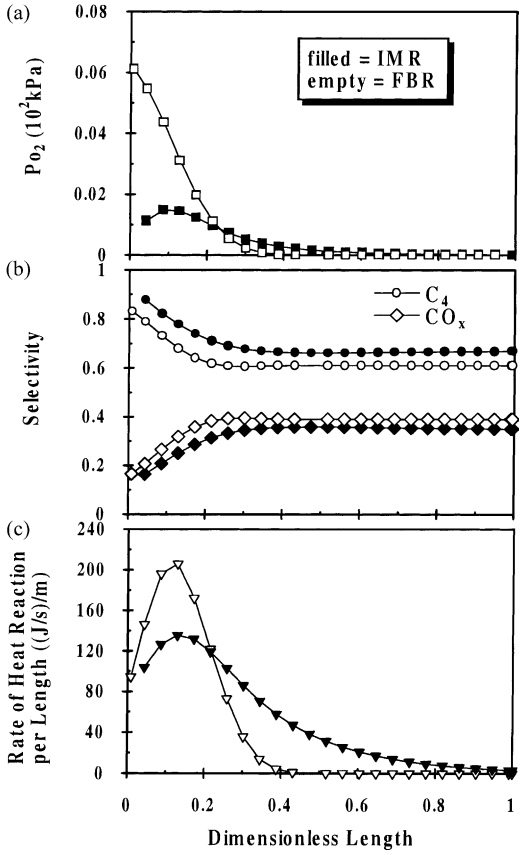

Fig. 7. Comparison of FBR and IMR: (a) partial pressure of oxygen in catalyst bed; (b) selectivity; (c) head of reaction (air/*n*-butane ratio = 8, $d = 0.006$ m, $L = 0.24$ m, feed flow rate of *n*-butane 1.653×10^{-5} mol/s, T_f and $T_j = 773$ K).

the hot spot where the temperature reaches to the maximum value can be found at the center of reactor.

The hot spot temperature from the plug flow model which has the temperature profile close to that near the wall in Fig. 6 (not shown) differs significantly from the radial diffusion model. Hence, the following studies will be carried out using the radial diffusion model.

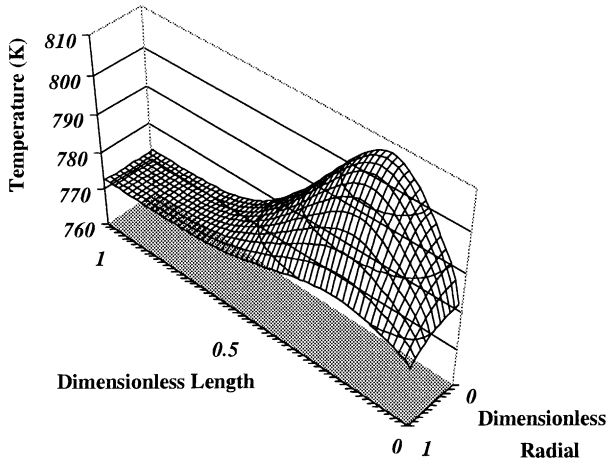

Fig. 6. Temperature profile in radial diffusion model (air/*n*-butane ratio = 7, $d = 0.006$ m, feed flow rate of *n*-butane = 1.653×10^{-5} mol/s, T_f and $T_j = 773$ K, $W/F_{C_4H_{10}} = 150$ kg s/mol).

3.2. Membrane reactor study

3.2.1. Comparison between fixed-bed reactor and membrane reactor

Fig. 7 compares the results of the fixed-bed reactor and the membrane reactor. It should be noted that in the membrane reactor the catalyst bed was packed in the annulus while in the fixed bed reactor the catalyst was packed in the tube side. It is obvious that the partial pressure of oxygen along the reactor length for the membrane reactor is smoother than that of the fixed-bed reactor. This is because the membrane is employed to distribute oxygen to the reaction chamber along the reactor length. The results also show one advantage on the selectivity improvement by using the controlled addition of oxygen to keep the partial pressure of oxygen at low value. As a result, complete oxidation to CO and CO_2 is suppressed. This phenomenon is also found in other systems such as oxidative coupling of methane [24]. Another point to be addressed is that due to lower amount of O_2 at the

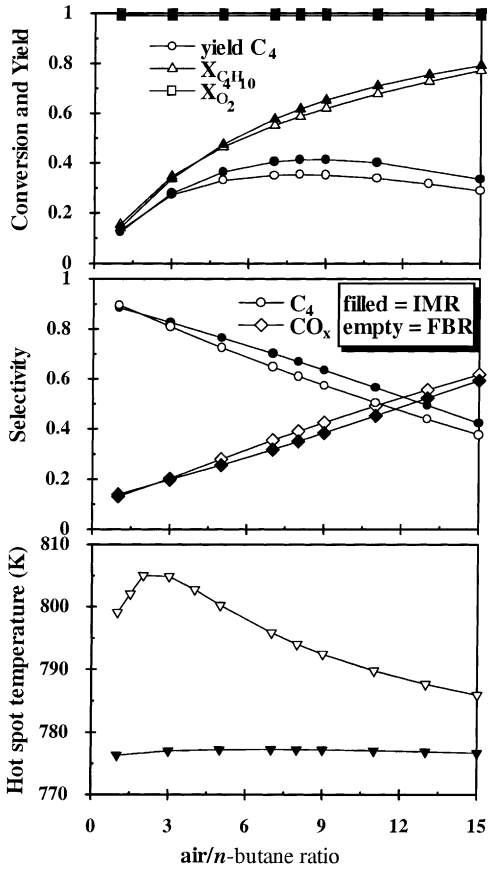

Fig. 8. Effect of air/*n*-butane ration to performance of reactor ($d = 0.006$ m, T_f and $T_j = 773$ K, $L = 0.24$ m).

entrance the heat of reaction for the membrane reactor is less severe than the fixed-bed reactor.

3.2.2. Effect of air to n-butane ratio

Fig. 8 compares the performance of the fixed-bed reactor and the membrane reactor at various ratio of air to *n*-butane. It can be seen that the increase of the ratio results in the increased conversion and decreased selectivity to butene and butadiene. At low value of the ratio, on the other words lower amount of oxygen, the conversion and selectivity for both reactors are almost the same. However, when the ratio increases the selectivity to the total dehydrogenated C_4 products of the membrane reactor becomes superior to that of the fixed-bed reactor. There is an optimum ratio where the yield to the total dehydrogenated C_4 is maximum, the ratio of 8 for the fixed-bed reactor and 9 for the membrane reactor. At low value of the ratio even though the selectivity is high but the conversion is low as the amount of oxygen is limited; however, at very high value of the ratio the reaction products are oxidized to form carbon oxides. It should be noted that another important advantage of the membrane reactor is the avoidance of hot spot. It was found that the hot spot temperature of the fixed-bed reactor is much higher than that of the membrane reactor independently of the feed ratio.

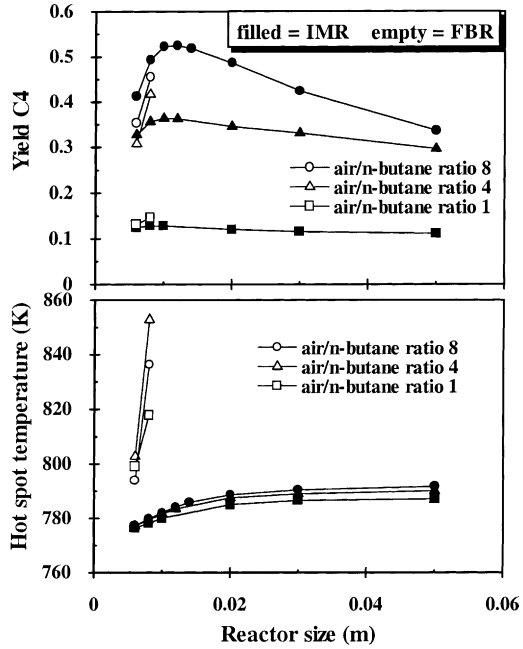

Fig. 9. Effect of reactor diameter on yield C_4 and hot spot temperature (air/*n*-butane ratio = 1, 4 and 8, T_f and $T_j = 773$ K, $L = 0.24$ m).

3.2.3. Effect of reactor diameter

Fig. 9 shows the effect of the reactor size to the performance of the reactors. The specification of the reactors at different size is summarized in Table 3. The increase of the reactor size while keeping the membrane surface area constant results in the increased amount of catalyst for the reaction; however, it is expected that the effect of radial dispersion should be more pronounced. For the fixed-bed reactors (FBR), the simulated results could not be obtained at larger than 0.01 m of reactor size for any feed ratios because the hot spot temperature was too high. On the other hand, for the inert membrane reactor (IMR), relatively small increase of the hot spot temperature is observed.

One interesting results found in this study is that there is an optimum reactor diameter of approximately 0.01 m where the yield of total dehydrogenated product C_4 is maximum. In the range of the reactor size smaller than the optimum value, the increase of the reactor size decreases the amount of catalyst which results in more reaction and more heat

Table 3
The reactor size in study[a]

Reactor size	Fixed-bed reactor		Membrane reactor	
	i.d. (m)	o.d. (m)	i.d. (m)	o.d. (m)
0.006	0.006	0.009	0.0117	0.0147
0.01	0.01	0.013	0.0141	0.0171
0.02	0.02	0.023	0.0224	0.0254
0.03	0.03	0.033	0.0316	0.0346
0.05	0.05	0.053	0.051	0.054

[a] The reactor size of inert membrane reactor was calculated based on the equivalent area of the reaction zone.

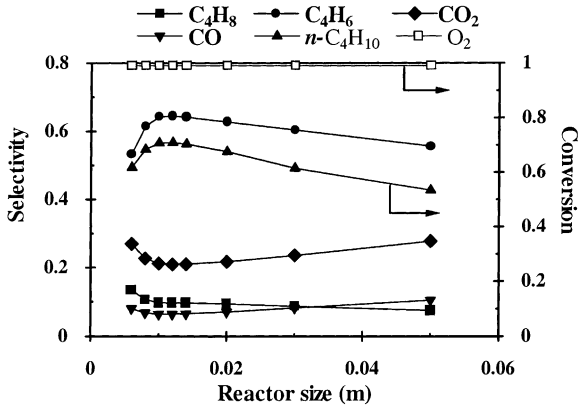

Fig. 10. Effect of reactor on selectivity and conversion (air/*n*-butane ratio = 8, feed flow rate of *n*-butane = 1.653×10^{-5} mol/s, T_f and $T_j = 773$ K, $L = 0.24$ m).

generation. The increased temperature increases conversion and selectivity to the product C_4. However, when considering the range of the reactor size larger than the optimum value the increased reactor size decreased the yield. This can be explained by considering Fig. 10 which shows the conversion and the selectivity for the case where the air/*n*-butane ratio is equal to 8. The oxygen conversion is 100% for all the reactor sizes. From the optimum value of the reactor size, when the reactor size increases, the conversion of *n*-butane decreases. It means that oxygen is consumed to oxidize the product to carbon oxides as found that the selectivity to butadiene and butene decreases while the selectivity to carbon dioxide and carbon monoxide increases. This can be explained that oxygen permeating to the reaction side cannot reach *n*-butane near the stainless steel wall due to the effect of radial dispersion (not shown).

3.2.4. Effect of reactor wall temperature

Fig. 11 shows the effect of wall temperature for both IMR and FBR. For both cases, with the increased wall temperature the yield of product C_4 becomes higher. For the fixed-bed reactor, the increase of wall temperature significantly increases the hot spot temperature. Conversely, relatively small increase of the hot spot temperature is observed in the membrane reactor. The results are similar to the effect of reactor size. It should be noted that for the case of fixed-bed reactor with reactor size of 0.012 m, the yield is very high, however, it results in much higher hot spot temperature which should be avoided in practical operation.

3.2.5. Effect of feed air temperature

Fig. 12 shows the effect of feed air temperature on the temperature profile along the reactor length in the membrane reactor. It is desirable to operate the reactor at small hot spot temperature to avoid subsequent problems such as catalyst deactivation and run-away reaction. The decrease of feed air temperature can reduce the hot spot temperature as the temperature profile becomes close to the isothermal

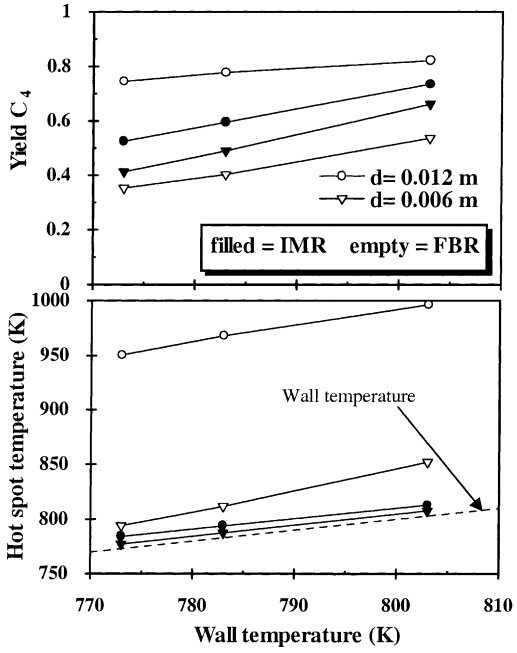

Fig. 11. Effect of wall temperature of fixed-bed reactor and membrane reactor (air/*n*-butane ratio = 8, feed flow rate of *n*-butane = 1.653×10^{-5} mol/s, $T_f = 773$ K, $d = 0.006$ and 0.012 m, $L = 0.24$ m).

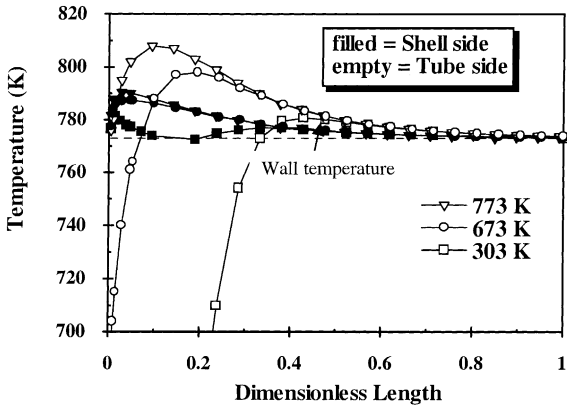

Fig. 12. Effect of feed air temperature on average temperature along the reactor length (air/*n*-butane ratio = 8, feed flow rate of *n*-butane = 1.653×10^{-5} mol/s, $W/F_{C_4H_{10}} = 7174$ kg/(mol/s), $T_{f,n\text{-butane}} = 773$ K, $T_j = 773$ K, $L = 0.24$ m).

condition. The heat of reaction which occurs mainly near the membrane surface can directly transfer to the cold feed air as found that the temperature in the tube side rapidly increases and reaches to the asymptote.

4. Conclusion

The oxidative dehydrogenation of *n*-butane in a porous membrane reactor was studied by mathematical modelling of a fixed-bed reactor and a membrane reactor. The non-isothermal condition and both radial heat and mass

dispersion were considered. It was found that the selectivity to C_4 hydrocarbon increased with the increasing operating temperature, and that the hot spot problem and the effect of radial dispersion were pronounced particularly near the entrance of the reactor. The use of the porous membrane to control the distribution of oxygen feed to the reaction side could significantly reduce the hot spot temperature. The results also showed that there were optimum feed ratios of air/*n*-butane for the fixed-bed reactors and the membrane reactors. The membrane reactor outperformed the fixed-bed reactor at high values of the ratio. In addition, there is an optimum membrane reactor size. When the reactor size was smaller than the optimum value, the increased reactor size increased the reaction and heat generation and, consequently, the conversion and the selectivity to C_4 increased. However, when the reactor size was larger than the optimum value, oxygen could not reach the reactant near the stainless steel wall. It was consumed to react with the product, C_4. As a result, the yield dropped. Finally, it was found that the increase of wall temperature increased the yield and that the feed air temperature could help control the temperature profile of the reaction bed along the reactor length.

Acknowledgements

The supports from TRF and TJTTP-OECF are gratefully acknowledged.

Appendix A

1. The viscosity of gas mixture at low pressure is shown below [25]:

$$\mu_{\mathrm{m}} = \sum_{i=1}^{n} K_i \left(1 + 2 \sum_{j=1}^{i-1} H_{ij} K_j + \sum_{j=1 \neq i}^{n} \sum_{k=1 \neq i}^{n} H_{ij} H_{ik} K_j K_k \right) \quad \text{(A.1)}$$

where the parameter K is the functions of molecular weight, mole fraction and viscosity of pure component and the parameter H_{ij} is the functions of polar correction, reduced dipole moment, molecular weight, etc.

2. Diffusion coefficient of mixture ($D_{i,\mathrm{m}}$) gas is calculated by the relation:

$$\frac{1 - y_i}{D_{i,\mathrm{m}}} = \sum_{j=1, j \neq i}^{n} \frac{y_j}{D_{ij}} \quad \text{(A.2)}$$

where D_{ij} = diffusion coefficient of binary gas (m^2/s).

3. The effective radial diffusion D_{er} is calculated by the relation [26]:

$$\frac{1}{Pe_{\mathrm{r}}} = \frac{0.4}{(Re_{\mathrm{p}} Sc) 0.8} + \frac{0.009}{\{1 + 10/(Re_{\mathrm{p}} Sc)\}} \quad \text{(A.3)}$$

for $0.4 < Re_{\mathrm{p}} < 500, 0.77 < Sc < 1.2$ where Pe_{r} = Peclet number, $ud_{\mathrm{p}}/D_{\mathrm{er}}$; Sc = Schmidt number, $\mu/\rho D_{i,\mathrm{m}}$; $Re_{\mathrm{p}} = \rho u d_{\mathrm{p}}/\mu_{\mathrm{m}}$.

4. Enthalpy of reaction and heat capacity are shown below:

$$\Delta H_{\mathrm{T}} = \Delta H_{298} + \int_{298}^{T} \Delta C_p \, \mathrm{d}T \quad \text{(A.4)}$$

where

$$\Delta C_p = \sum_i \nu_i C_{pi} \quad \text{(A.5)}$$

and

$$\frac{C_{pi}}{R_{\mathrm{gas}}} = A + BT + CT^2 + ET^3 + DT^{-2} \quad \text{(A.6)}$$

where $R_{\mathrm{gas}} = 8.314\,\mathrm{J\,mol^{-1}\,K^{-1}}$.

The standard heat of formation at 298 K and the constant A, B, C and D are shown in Table 4 [27].

5. The overall heat transfer coefficient

In this case, we assume the film heat transfer between reactor surface and external fluid is negligible.

For fixed bed reactor:

$$\frac{1}{U_{\mathrm{ss}} A_{\mathrm{P1}}} = \frac{1}{h_{\mathrm{bed}} A_{\mathrm{P1}}} + \frac{\ln(r_2/r_1)}{2\pi k_{\mathrm{ss}} L} \quad \text{(A.7)}$$

$$A_{\mathrm{P1}} = 2\pi r_1 L$$

Table 4
Heat of formation and heat capacities of gases

Chemical species	H^0_{298} (kJ/mol)	$T_{\max}$ (K)	A	$10^3 \times B$	$10^6 \times C$	$10^{-6} \times E$	$10^{-5} \times D$
n-C_4H_{10}	−125.79	1500	1.935	36.915	−11.402	–	–
1-C_4H_8	−0.54	1500	1.967	31.63	−9.873	–	–
t-C_4H_8	−10.06	1500	1.085	36.621	−17.377	0.0134	–
c-C_4H_8	−5.7	1500	−0.958	40.726	−20.447	0.0142	–
C_4H_6	109.24	1500	2.734	26.786	−8.882	–	–
O_2	0	2000	3.639	0.506	–	–	−0.227
CO	−110.53	2500	3.376	0.557	–	–	−0.031
CO_2	−393.51	2000	5.457	1.045	–	–	−1.157
H_2O	−241.82	2000	3.47	1.45	–	–	0.121
N_2	0	2000	3.28	0.593	–	–	0.04

where h_{bed} [28] and k_{ss} [29] is calculated by the following relation:

$$Nu_{bed} = \frac{h_{bed} d_p}{\lambda_g} = 5Re_p^{0.365} \quad (A.8)$$

$$k_{ss} = -5 \times 10^{-6} T^2 + 0.0215T + 9.0303 \quad (A.9)$$

For membrane reactor:

$$\frac{1}{U_{ss} A_{P3}} = \frac{1}{h_{bed} A_{P3}} + \frac{\ln(r_4/r_3)}{2\pi k_{ss} L} \quad (A.10)$$

$$A_{P3} = 2\pi r_3 L$$

And overall heat transfer coefficient through membrane is shown in the followings:

$$\frac{1}{U_M A} = \frac{1}{h_{bed} A_{P1}} + \frac{\ln(r_2/r_1)}{2\pi k_M L} + \frac{1}{A_{P2} h_{ex}} \quad (A.11)$$

where $A_{P1} = 2\pi r_1 L$; $A_{P2} = 2\pi r_2 L$ and h_{ex} and k_M is calculated by the following relation [29,30]:

$$Nu_{ex} = \frac{h_{ex} D}{\lambda_g} = 3.66 + \frac{0.0668(D/L)RePr}{1 + 0.04[(D/L)RePr]^{2/3}} \quad (A.12)$$

$$k_M = 111058(T)^{-1.3867} \quad (A.13)$$

6. The heat thermal conductivity of mixture gas is shown in the following expression [25]:

$$\lambda_m = \sum_{i=1}^{n} \frac{y_i \lambda_i}{\sum_{j=1}^{n} y_j A_{ij}} \quad (A.14)$$

The parameter A_{ij} is calculated from monatomic values of thermal conductivity and molecular weight.

7. The effective radial thermal conductivity λ_{er} on the catalyst bed is calculated by the relation [31]:

$$\lambda_{er} = \lambda_{er}^0 + \lambda_{er}^t \quad (A.15)$$

The effective radial thermal conductivity is considered to consist of two contributions, the first static that is the effective thermal conductivity of the quiescent bed and the second is the dynamic contribution (i.e. dependent on the flow conditions), so that

$$\lambda_{er}^0 = f(\lambda_m, \varepsilon, \lambda_s) \quad (A.16)$$

$$\lambda_{er}^t = \varepsilon \rho C_p D_{er} \quad (A.17)$$

References

[1] R. Soria, Overview on industrial membranes, Catal. Today 25 (1995) 285–290.

[2] N.J. Armor, Application of catalytic inorganic membrane reactors to refinery products, J. Memb. Sci. 147 (1998) 217–233.

[3] V.M. Gryaznov, Membrane catalysis, Catal. Today 51 (1999) 391–395.

[4] J. Santamaria, J. Coronas, Catalytic reactors based on porous ceramic membranes, Catal. Today 51 (1999) 377–389.

[5] G. Saracco, H.W.J.P. Neomagus, G.F. Versteeg, W.P.M. Van Swaaij, High-temperature membrane reactors: potential and problems, Chem. Eng. Sci. 54 (1999) 1997–2017.

[6] G. Capannelli, E. Carosini, O. Monticelli, Enhancement of the catalytic performance of V_2O_5/γ-Al_2O_3 catalysts in the oxidehydrogenation of propane to propylene by the use of a monolith-type reactor, Catal. Lett. 39 (1996) 241–246.

[7] G. Capannelli, E. Carosini, F. Cavani, O. Monticelli, F. Trifiro, Comparison of the catalytic performance of V_2O_5/γ-Al_2O_3 in the oxidehydrogenation of propane to propylene in different reactor configuration: (i) packed-bed reactor; (ii) monolith-like reactor and (iii) catalytic membrane reactor, Chem. Eng. Sci. 51 (1996) 1817–1826.

[8] M.J. Alfonso, A. Julbe, D. Farrusseng, M. Menendez, J. Santamaria, Oxidative dehydrogenation of propane on V/γ-Al_2O_3 catalytic membranes. Effect of the type of membrane and reactant feed configuration, Chem. Eng. Sci. 54 (1999) 1265–1272.

[9] M.J. Alfonso, M. Menendez, J. Santamaria, Vanadium-based catalytic membrane reactors for the oxidative dehydrogenation of propane, Catal. Today 56 (2000) 247–252.

[10] R. Ramos, M. Menendez, J. Santamaria, Oxidative dehydrogenation of propane in an inert membrane reactor, Catal. Today 56 (2000) 239–245.

[11] J. Coronas, M. Menendez, J. Santamaria, Use of a ceramic membrane reactor for the oxidative dehydrogenation of ethane to ethylene and higher hydrocarbons, Ind. Eng. Chem. Res. 34 (1995) 4229–4234.

[12] A.L.Y. Tonkovich, R.B. Secker, E.L. Reed, G.L. Roberts, J.L. Cox, Membrane reactor/separator: a design for bimolecular reactant addition, Sep. Sci. Technol. 30 (1995) 1609–1624.

[13] A.L.Y. Tonkovich, J.L. Zilka, D.M. Jimenez, L. Gary, Experimental investigations of inorganic membrane reactors: a distributed feed approach for partial oxidation reactions, Chem. Eng. Sci. 51 (1996) 789–806.

[14] C. Tellez, M. Menendez, J. Santamaria, Simulation of an inert membrane reactor for the oxidative dehydrogenation of butane, Chem. Eng. Sci. 54 (1999) 2917–2925.

[15] C. Tellez, M. Menendez, J. Santamaria, Oxidative dehydrogenation of butane using membrane reactors, AIChE. J. 43 (1997) 777–784.

[16] J. Coronas, A. Gonzalo, D. Lafarga, M. Menendez, Effect of the membrane activity on the performance of a catalytic membrane reactor, AIChE 43 (11) 3095–3104.

[17] S. Assabumrungrat, P. Praserthdam, S. Goto, Oxidative coupling of methane in a ceramic membrane reactor: uniform oxygen permeation pattern, J. Chin. Institute Chem. Eng. 31 (1) 19–25.

[18] S. Cheng, X. Shuai, Simulation of a catalytic membrane reactor for oxidative coupling of methane, AIChE 41 (6) 1598–1601.

[19] M. Pedernera, R. Mallada, M. Menendez, J. Santamaria, Simulation of an inert membrane reactor for the synthesis of maleic anhydride, AIChE 46 (12) 2489–2498.

[20] M.A. Pena, D.M. Carr, K.L. Yeung, A. Varma, Ethylene epoxidation in a catalytic packed-bed membrane reactor, Chem. Eng. Sci. 53 (22) 3821–3834.

[21] C. Tellez, M. Menendez, J. Santamaria, Kinetic study of the oxidative dehydrogenation of butane on V/MgO catalysts, J. Catal. 183 (1999) 210–221.

[22] S. Assabumrungrat, D.A. White, Permeation of acetone and isopropanol vapours through a porous alumina membrane, Chem. Eng. Sci. 53 (1998) 1367–1374.

[23] A.A. Lemonidou, G.J. Tjatjopoulos, I.A. Vasalos, Investigations on the oxidative dehydrogenation of *n*-butane over VMgO-type catalysts, Catal. Today 45 (1998) 65–71.

[24] D. Lafarga, J. Santamaria, M. Menendez, Methane oxidative coupling using porous ceramic membrane reactors II. Reaction studies, Chem. Eng. Sci. 12 (1994) 2015–2025.

[25] R.C. Reid, J.M. Prausnitz, B.E. Poling, The Properties of Gases and Liquids, McGraw-Hill, New York, 1988.

[26] N. Itoh, W.C. Xu, K. Haraya, Radial mixing diffusion of hydrogen in a packed-bed type of palladium membrane reactor, Ind. Eng. Chem. Res. 33 (1994) 197–202.
[27] J.M. Smith, H.C. Van Ness, Introduction to Chemical Engineering Thermodynamics, McGraw-Hill, New York, 1987.
[28] M.K. Koukou, G. Chaloulou, N. Papayannakos, N.C. Markatos, Mathematical modelling of the performance of non-isothermal membrane reactors, Int. J. Heat Mass Transfer. 40 (1997) 2407–2417.
[29] A.F. Mills, Basic Heat and Mass Transfer, 1995.
[30] F.P. Incropera, D.P. De Witt, Fundamentals of Heat and Mass Transfer, Wiley, New York, 1990.
[31] G.F. Froment, K.B. Bischoff, Chemical Reactor Analysis and Design, Wiley, New York, 1990.